Measurement Science
and Technology

PAPER • **OPEN ACCESS**

Experimental and theoretical investigation of optical transmittance in light-transmitting concrete

To cite this article: Karina Hwang Arcolezi *et al* 2026 *Meas. Sci. Technol.* **37** 195201

Measurement Science and Technology

PAPER

Experimental and theoretical investigation of optical transmittance in light-transmitting concrete

Karina Hwang Arcolezi[1,2], **Camila Aparecida Zimmermann**[2], **Bora Ung**[2,*] and **Claudiane Ouellet-Plamondon**[1,*]

[1] Department of Construction Engineering, École de technologie supérieure, Montreal QC H3C 1K3, Canada
[2] Department of Electrical Engineering, École de technologie supérieure, Montreal QC H3C 1K3, Canada
[*] Authors to whom any correspondence should be addressed.

E-mail: bora.ung@etsmtl.ca and claudiane.ouellet-plamondon@etsmtl.ca

Keywords: optical transmittance measurement, ambient light, photodetector, smart concrete

OPEN ACCESS

RECEIVED
26 January 2026

REVISED
5 March 2026

ACCEPTED FOR PUBLICATION
27 April 2026

PUBLISHED
12 May 2026

Abstract

Light-transmitting concrete (LTC) is a cement-based composite that incorporates optical fibers to allow light transmission through cementitious composites elements, enabling architectural lighting. Despite growing interest in its optical performance, LTC lacks standardized procedures for measuring light transmittance, particularly concerning the distance between the specimen and the photodetector. This study addresses this gap by introducing a physical model based on a super-Gaussian intensity distribution to describe the light behavior emitted from embedded optical fibers. The model is validated through experimental tests using 5 cm cubic LTC specimens with up to 16 fibers and detector distances from 1 to 20 cm. The results reveal a nonlinear relationship between detector distance and measured transmittance, with an optimal detection distance observed around 5 cm for the investigated configurations. Specifically, for the 16-fiber configuration, the peak transmittance reached 0.33% at the optimal distance, which is higher than the 0.23% recorded at 1 cm or the 0.17% at 20 cm. Based on these findings, a practical predictive rule is proposed, linking this optimum to the fiber's numerical aperture and the specimen's dimensions. By providing a physically grounded framework for reliable optical transmittance measurements, the proposed approach highlights the potential of LTC for use in functional and smart concrete systems. Moreover, it contributes to the standardization of measurement procedures, enabling more consistent and reproducible evaluations of LTC performance in both research and industrial contexts.

1. Introduction

Light-transmitting concrete (LTC) and other cement-based composites are gaining recognition as materials that incorporate translucent or light-guiding components capable of transmitting light through the cementitious matrix [1–4]. These properties support applications in architectural design, integrated lighting systems, and sustainability-focused construction [1, 5]. Beyond its aesthetic appeal, LTC's ability to harness natural light can help reduce energy consumption from artificial lighting, thereby reinforcing interest in its optical behavior [6–9]. More broadly, cement-based composites incorporating optical fibers have been described in the literature as systems with passive or active optical behavior [10]. In passive configurations, such as conventional LTC, optical fibers guide light through the cementitious matrix, and optical transmittance is used to characterize the material's optical response. In active configurations, optical fibers are integrated into systems that enable interaction with external stimuli, supporting functionalities such as sensing, signal transmission, or image-related applications [11].

The efficacy of light transmission in LTC depends on parameters such as the diameter and content ratio of optical fibers [12–15], the spatial distribution of fibers and their density within the composite [15–18], characteristics of the light source, such as wavelength and power [8, 14, 19, 20], the numerical aperture (NA) of the optical fibers [7, 21, 22], and the distance between the sample and the detector

[19, 20, 23]. Owing to the large number of variables involved in the light transmittance measurements of LTC, there is considerable variation in the methodologies used in the scientific literature. This variability limits the comparability of reported results and affects the assessment of cement-based composites with optical fibers in both passive and active configurations. In this work, we theoretically and experimentally study the main parameters that influence light transmittance measurements of LTC with optical fibers and identify conditions that support more consistent and reproducible measurement procedures.

Light transmission in optical fiber-based LTC is enabled by the inclusion of optical fibers within a cementitious matrix [1]. Studies have consistently shown that increasing the optical fiber content and diameter tends to enhance light transmittance [12, 15], while an increase in the distance between the sample and the photodetector leads to a reduction in transmission due to light dispersion [12, 13, 15, 24, 25]. Despite these well-established trends, light transmittance measurement in optical fiber LTC lacks standardization, leading researchers to adopt diverse testing methods across studies [26, 27]. The absence of standardized methods for measuring detector-sample distance constitutes a significant gap in the field that the present study aims to address.

Experimental studies have highlighted the influence of detector distance on transmittance measurement results. Rong *et al* [24], in their investigation of LTC wall panels, observed that light intensity decreased from a measured peak of 46 lux to 11.8 lux as the distance from the sample and the light meter increased from 10 cm to 50 cm, regardless of the fiber configurations tested. Similarly, Robles *et al* [28] reported a gradual decrease in optical power, with increasing detector distance, with a more pronounced effect at distances between 0 and 100 mm. They found that at distances greater than 10 cm, the optical power ratios for LTC samples with different fiber diameters converged, suggesting that the impact of fiber diameter on transmittance diminishes at larger distances.

Consistent trends have also been reported for different fiber diameters and sample geometries. Nam *et al* [14] reported a significant decrease in light intensity, as the detector distance increased from 10 cm to 30 cm when analyzing samples with fiber diameters from 0.75 mm to 1.5 mm. The authors found that while larger fibers allowed higher initial power, they were also more susceptible to light dispersion over longer distances. Notably, fibers with a large diameter of 1.5 mm exhibited the highest power at any given distance, but experienced the highest drop as the detector moved farther from the sample, with an average light power reduction from approximately 100 μW at 10 cm to 10 μW at 30 cm. Tuaum *et al* [29] investigated the effect of detector distance on light transmittance in LTC by measuring light intensity through samples with 2 mm and 3 mm diameter optical fibers at distances from 10 to 50 cm. They found that transmittance decreased by increasing the detector distance. For 2 mm fibers with a 6% volume fraction, transmittance decreased from approximately 22% at 10 cm to approximately 12% at 50 cm. For 3 mm fibers, under similar conditions, transmittance decreased from approximately 19% at 10 cm to approximately 10% at 50 cm. These studies collectively reinforce the sensitivity of the measured optical output to detector-sample distance, highlighting the need for a clearer understanding of how this parameter affects reported values.

Despite the recognized effect of detector-sample distance on transmittance measurements, this parameter is still treated empirically, often lacking explicit physical justification or a standardized criterion for detector placement. As a result, measurement distances are frequently selected based on experimental convenience rather than on optical propagation considerations. The present work addresses this gap by introducing a predictive framework for detector placement based on super-Gaussian beam propagation. This approach correlates the optimal detection distance with sample geometry and fiber NA, providing a physically grounded basis for optical measurements in LTC.

Building on the identified gap in light-transmission measurements, this study aims to address the following research question: how does the distance between the light detector and the light-transmitting specimen influence the detected light power, and what is the optimal distance for reliable transmission measurements?

By integrating a theoretical model of light distribution from embedded fibers [30, 31] with experimental evaluations of LTC samples across varying fiber volume fractions, this work aims to quantify the relationship between detector positioning and measured optical power. The objective is to identify a stable distance range that ensures representative and reproducible transmittance measurements. Ultimately, this research establishes a physically grounded methodology for the optical characterization of LTC, providing a consistent basis for evaluating both passive and optically active configurations in smart concrete research.

Table 1. Specifications of PMMA optical fiber.

Core material	Polymethyl-methacrylate resin
Core diameter	0.92–1.04 mm
Core refractive index	1.49
Cladding material	Fluorinated polymer
Cladding diameter	0.94–1.06 mm
Cladding refractive index	1.40
Refractive index profile	Step-index
Numerical aperture	0.5
Attenuation at 650 nm	$\leqslant$0.0002 dB mm^{-1}
Operation temperature	−55 °C–70 °C
Tensile strength	83 MPa

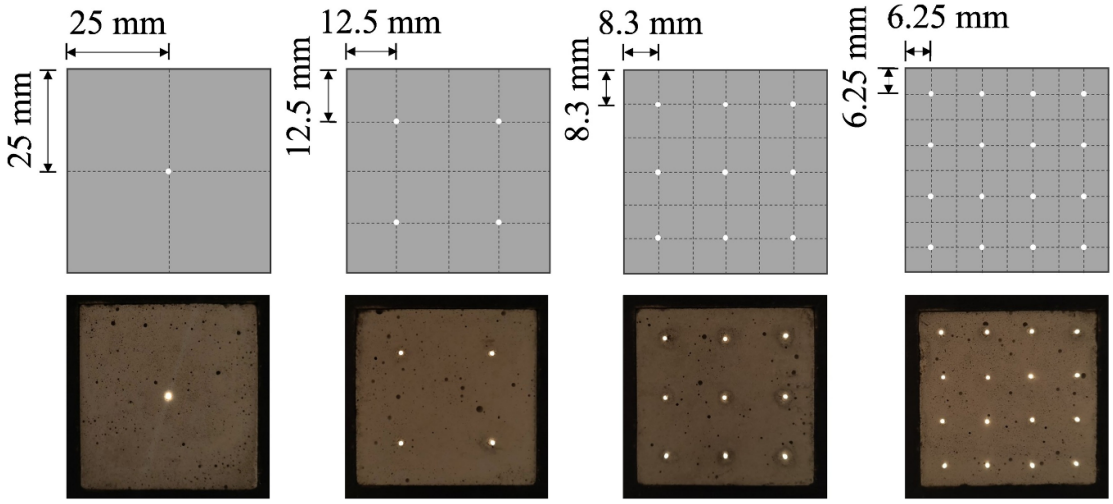

Figure 1. Distribution of optical fibers embedded in LTC samples. Fibers are shown for configurations with different numbers of fibers (N = 1, 4, 9, 16).

2. Materials and methods

2.1. LTC samples preparation

Samples of LTC with different quantities of optical fibers were fabricated and analyzed. The cementitious matrix was inspired by limestone-calcined clay cement. Ordinary Portland Cement (type GU, conforming to CSA A3000 standards [32]) served as a primary binder, supplemented with calcined clay and limestone filler, and natural river sand as fine aggregate, and a polycarboxylate-based superplasticizer. The mortar cube production method followed the approach described by Arcolezi *et al* [33] and Jin *et al* [34]. The optical fibers used in this study are made of polymethyl-methacrylate (PMMA) with a core diameter of 1 mm, featuring high transparency in the visible spectrum suitable for light guiding [35, 36]. Table 1 summarizes the properties of the PMMA fiber used (Eska^{TM}).

To minimize misalignment losses, fibers were threaded through rigid, precision-drilled formwork plates at both the input and output faces of the cubic molds. This ensured the fiber longitudinal axes remained perpendicular to the concrete surface and parallel to the incident light source, thereby reducing coupling losses associated with the fibers' acceptance cone [1].

Cubic LTC samples of 5 cm side length were used to evaluate the influence of fiber quantity on light transmittance. Optical fibers were arranged in a square lattice pattern to provide a standardized, reproducible geometric baseline for validation against the theoretical model. While other distributions (e.g. random or hexagonal packing) are possible, the square arrangement simplifies the geometric variables required for the model. The number of fibers in a sample progressively increased, from a single fiber to 4, 9, and 16 fibers. Figure 1 illustrates the fiber distribution within the various samples and the corresponding photographs for each configuration.

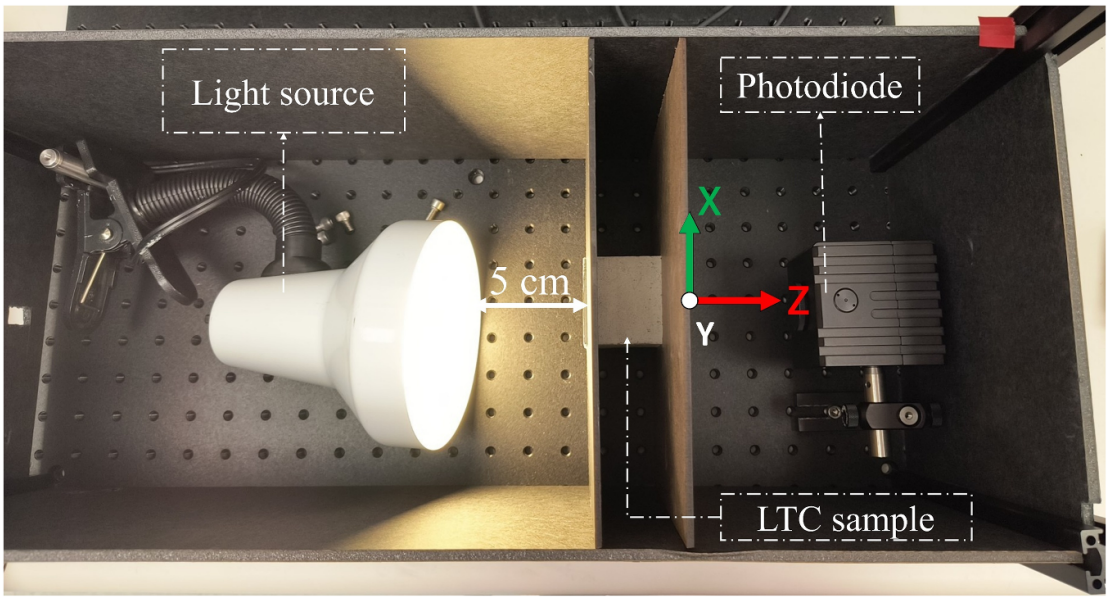

Figure 2. Experimental setup for light transmission measurements, showing the sample, light source, and detector (top cover removed for clarity).

2.2. Light transmission analysis

Light transmittance tests were conducted within a matte black cardboard enclosure to minimize reflections of light on the inner walls that would otherwise contaminate the measurements [21]. To ensure that only light passing through the fibers was measured while effectively blocking ambient light, two walls were constructed around the specimen to prevent light leakage (figure 2). A 6 W LED light bulb with a peak wavelength of 600 nm and a high-power RGB LED with peak wavelengths of 630 nm, 528 nm, and 465 nm were employed as light sources. Each color channel of the RGB LED was calibrated to a constant output intensity (3 W per channel) to ensure consistency across wavelengths, enabling accurate comparison of light transmittance. All experiments were conducted in a standard room temperature and humidity (around 21 °C and 40% relative humidity) in a laboratory environment to prevent variability from external environmental factors. These conditions are comfortably within the operating range specified for PMMA fibers in table 1, ensuring that their optical behavior remains unchanged during testing. The cementitious matrix is also not expected to undergo any measurable variation in optical response under such mild and stable environmental conditions.

To characterize the spectral distribution of the transmitted light, the spectrum of each light source was measured using an optical spectrometer (HR4000CG, Ocean Optics Inc.), while optical power measurements were performed using an integrating sphere photodiode (S142C, Thorlabs Inc.) connected to a power meter interface (PM100USB, Thorlabs Inc.). The distance between the light source and the sample was fixed at 5 cm to ensure uniform illumination conditions across the entire 50 × 50 mm^2 sample face throughout the experiment. The photodetector was centered both vertically and horizontally with respect to the sample, and the distance between them (figure 2, z-axis) was systematically varied to assess its impact on the transmittance measurements and determine the optimal distance.

The photodiode features a 12 mm input diameter aperture, which is substantially smaller than the specimen's output surface. Since the detector samples are only a portion of the emerging light beam, the measured signal depends not only on the total transmitted power but also on how the light is distributed across the sample's exit face. Optimization of the sample-detector distance is required to identify the location where this specific aperture size captures a stable and representative fraction of the non-homogeneous light distribution from the fiber array, improving the consistency of the transmittance measurements.

The initial light power (P_0) was recorded each time the specimen or the distance between the specimen and the photodiode was modified, to ensure a consistent reference P_0 value. Additionally, a control specimen (without optical fiber) was tested to confirm that the photodiode reading was 0 μW (perfectly opaque), thereby verifying that the walls effectively blocked external light and that no light leaked

around the sample's edges. For each testing configuration, two samples were evaluated for light transmittance, and each measurement was performed twice to verify the stability of the signal. The average value was calculated to ensure consistency and repeatability of the measurements.

The light transmittance (T), in units of %, was calculated using equation (1), by comparing the reference power from the light source (P_0) with the light power transmitted after passing through the sample (P_1) in μW units:

$$T = \frac{P_1}{P_0} \times 100. \tag{1}$$

The theoretical model of transmittance of the LTC needs to consider the specific properties of both the cementitious sample and the optical fibers that it contains. The optical fibers used in this study have a specified attenuation of 0.002 dB cm^{-1} at 650 nm. This loss can be converted to a transmission percentage using the expression $k = 100 \times 10^{\left(-\frac{\alpha L}{10}\right)}$, where k is the attenuation factor, α is the transmission loss coefficient in dB cm^{-1}, and L is the optical fiber length in cm [22]. For an optical fiber length of 5 cm, this attenuation yields a theoretical fiber transmission of $T_{\text{Fiber}} = 99.8\%$ of the light incident on the fiber core at the entrance facet. The maximum theoretical transmittance of the sample can be estimated by summing up the transmission efficiency of the optical fibers with their contribution to the total surface area of the specimen. Specifically, the max theoretical transmittance (T_{max}) is defined as the total cross-sectional area of the fibers, multiplied per the number of fibers ($S_{\text{Fiber}} \times N$), times the fiber transmission, over the total surface area of the sample (S_{Sample}), as described in equation (2),

$$T_{\text{max}}(\%) = \frac{(S_{\text{Fiber}} \times N) \times T_{\text{Fiber}}}{S_{\text{Sample}}}. \tag{2}$$

2.3. Determination of the optimal distance between the sample and the detector for power detection optimization

To determine the optimal testing distance between the LTC sample and the photodetector, a theoretical model of light transmittance was developed that incorporates parameters such as the light source characteristics, the NA of the optical fibers, and the sample dimensions. The NA defines the light acceptance angle of the fiber and depends on the refractive indices of the core and cladding [7]. This model assumes the use of multimode optical fiber with a step-index refractive profile, which is commonly employed in light-transmitting applications owing to their large surface area and power handling [31]. These fibers typically emit a light beam whose profile is nearly Gaussian in shape. The super-Gaussian profile is chosen for the model because it better accounts for the more complex light distribution seen in multimode fibers [31, 37]. In fact, the super-Gaussian distribution captures the effects of both beam divergence and intensity decay over the distance from multimode fibers more accurately, compared to single-mode fibers where a standard Gaussian beam profile model would be more suitable [30, 37].

The general form of the super-Gaussian intensity profile as a function of radial distance r (m) from the beam center is given by equation (3) [30],

$$I(r,z) = I_0 \cdot \exp\left(-2\left(\frac{r}{w(z)}\right)^n\right). \tag{3}$$

Where $I(r)$ is the intensity at radius r (W m^{-2}), I_0 is the peak intensity in W minus^{-2}, and w is the beam radius (m) which grows with propagation distance as $w(z) = z \cdot \tan\theta + w_0$. In the last expression, we note that the radius of the initial beam width (w_0) is taken as the core radius of the optical fiber (0.5 mm) and the divergence angle θ of light output from an optical fiber is given by $\theta = \sin^{-1}(\text{NA})$. For $n = 1$, the profile corresponds to a conventional Gaussian distribution, while the expression with $n > 1$ describes a flatter and sharper beam profile [37]. The beam shape is an important element that determines the light distribution and intensity received by the detector [31]. The input power P (in μW) from the light source is distributed over the cross-sectional area of the beam, leading to the peak intensity I_0 at the center of the beam (in μW cminus^{-2}). This peak intensity is calculated assuming a uniform power distribution over a circular cross-section with radius w (cm^2), and given by $I_0 = \frac{P}{\pi w^2}$.

The beam divergence from a single optical fiber generates a conical beam profile where the light spreads symmetrically around the propagation axis (figure 3). As the beam radius increases with distance, the intensity of the light decreases due to the distribution of optical power over a larger area. The incorporation of N fibers thus yields N conical beams of light that overlap, resulting in regions of

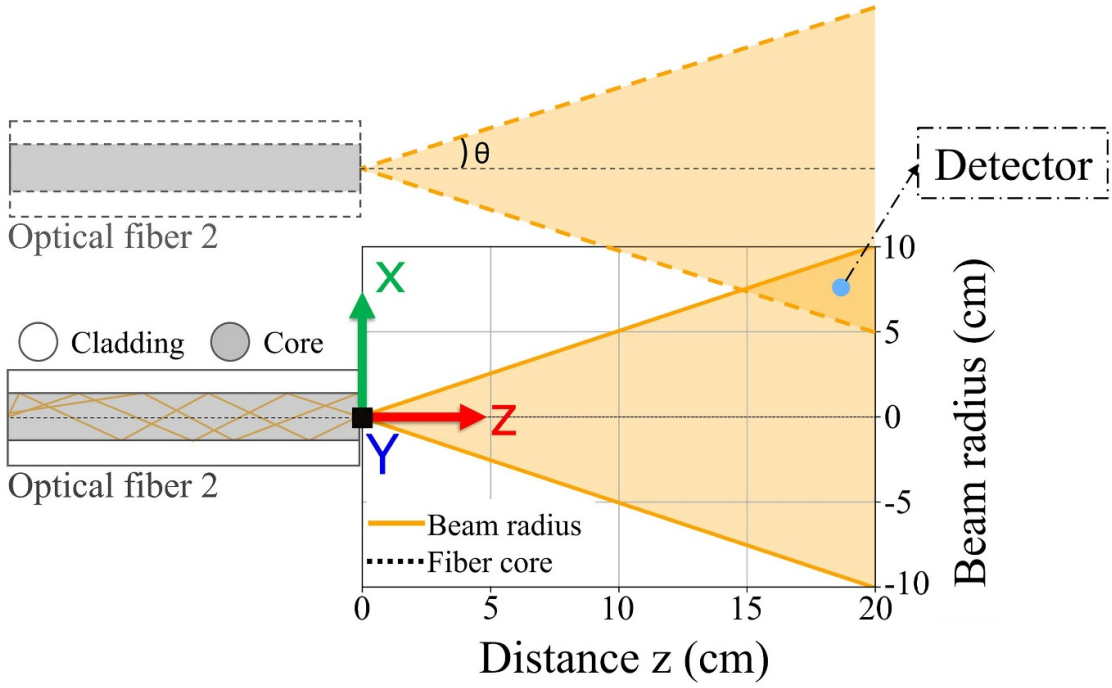

Figure 3. Conical beam profiles from optical fibers and their overlap, illustrating the region of intensified light intensity for optimized power detection.

higher light intensity, as well as darker regions in areas between adjacent fibers (figure 3). This highlights the importance of properly choosing the location of the photodetector to maximize light detection. Assuming that the N fibers are evenly distributed on the surface of a given LTC sample, the optimal location of the photodetector that best approximates the overall LTC transmittance will be aligned with the center of the sample and located at a distance z that maximizes the amount of transmitted light measured at the detector. Such optimal detector position should enhance the accuracy and reliability of power detection and transmittance measurements in the evaluation of fiber-based LTC samples.

The model simulates the power detection efficiency of the beam as it exits the optical fiber and propagates through free space. The objective is to quantify the percentage of light power detected by a circular detector positioned at varying distances from the fiber while accounting for attenuation over a specific fiber length. The model integrates the power detected by the circular photodetector (diameter of 12 mm) at a given distance z from the center of the sample's output surface. The optical power measured by the circular detector (P_{detector}) is computed by integrating the total light intensity produced by the N super-Gaussian beams (output from the N fibers) over the detector's area (A_{detector}) via the double integral in equation (4), where the integration bounds along the x and y coordinates are defined by the detector's dimensions in the x–y directions (figure 3). The theoretical model focuses on square lattice fiber configurations to simplify the initial complexity of the multi-fiber system and establish the fundamental geometric criteria for light distribution analysis,

$$P_{\text{detector}}(z) = \iint_{A_{\text{detector}}} \left[\sum_{i=1}^{N} I_i(r,z)\right] \mathrm{d}x\mathrm{d}y\,. \tag{4}$$

The modeling approach incorporates a geometric criterion to define the optimal measurement position. This criterion is based on the hypothesis that the ideal distance corresponds to the point where the expanding light cones, originating from the outermost fibers, begin to overlap at the detector plane. At this specific distance, the detector is expected to record a portion of the emerging field that best represents the total transmitted power. This geometric principle, which considers the beam divergence characteristics and the dimensions of the optical arrangement, provides the physical basis for the predictive rule developed in this study.

Subsequently, the fraction of power detected in watts at each distance z (cm) is evaluated. By simulating the beam profile at different distances, considering factors such as beam divergence, detector offset, and fiber attenuation, this theoretical model (equations (3) and (4)) provides a physically accurate

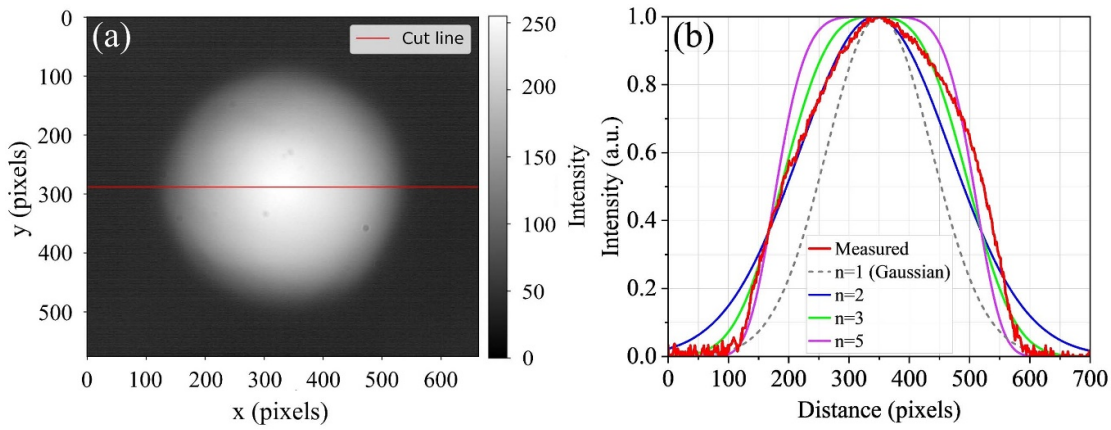

Figure 4. Comparison of (a) measured beam profile and (b) intensity distribution compared with super-Gaussian models for different n values.

description and enables a systematic investigation of an optimal detection distance for light transmittance studies in LTC samples.

3. Results and discussions

3.1. Beam profile and transmittance analysis

Parameter n for the super-Gaussian model was determined by comparing the experimental beam profile, captured using a visible camera (EO-0413M CMOS monochrome, Edmund Optics), to theoretical profiles simulated for various values of n. The output beam profile from an optical fiber was experimentally measured at a distance $z = 30$ cm (from the fiber output), shown in figure 4(a). The measured beam profile was analyzed by extracting its intensity distribution along a cross-sectional line (red line in figure 4(a)) through the optical beam's center and presented in figure 4(b) as the solid red curve. Several theoretical profiles ($n = 1$, 2, 3, and 5) of super-Gaussian beams (see equation (3)) were compared. The Gaussian profile ($n = 1$) is narrower than the measured beam, underestimating the width of the emission. The profile with $n = 2$ better represents the peak intensity but remains slightly narrower than the actual distribution. The curve with $n = 3$ provided the best overall agreement, capturing both the peak and the broader intensity tails of the measured beam. Higher values of n, such as 5, produced profiles with very sharp edges resembling a top-hat distribution [37–39] that could be suited for other types of multimode fibers, such as with larger core diameters for example.

The arrangements of optical fibers for each LTC sample are detailed in figure 1. Figure 5 displays the modeled beam profile for a single fiber centrally positioned, and as a function of distance z, where the blue circle at the center represents the detector. In this special configuration ($N = 1$), there is no obvious optimal distance since the detected light power is maximum at $z = 0$ and simply decays with the distance $z > 0$. Still, the modeled beam profiles in figure 5 highlight the beam divergence phenomenon (and expanding beam profiles) with increasing distance from the fiber output [37].

For samples with multiple optical fibers ($N > 1$), there is an optimal distance for the detector where the measured optical power is maximum. For the four-fiber sample, the analysis also considers optical fiber offsets relative to the center of the specimen. In this setup, positioning the detector too close to the specimen (i.e. at $z = 0$ or 1 cm in figure 6) may result in failure to detect any light power emitted from the light cones, since the center of the sample does not contain any fiber. As the distance increases, the light cones expand, allowing the center-aligned detector to capture more power (figure 6). There is thus potentially an optimal distance z at which to position the detector so as to maximize light collection, as we will see in the next section.

In the nine-fiber configuration ($N = 9$), a central fiber aligns with the detector. If considering only this central fiber, the optimal detection distance would place the detector as close as possible to capture its light output (i.e. $z = 0$). However, the additional eight fibers complicate this arrangement. For effective detection of the maximum overlap intensity from all nine fibers, the detector must be positioned farther away. As seen in figure 7, increasing the distance from the sample allows the light cones from all

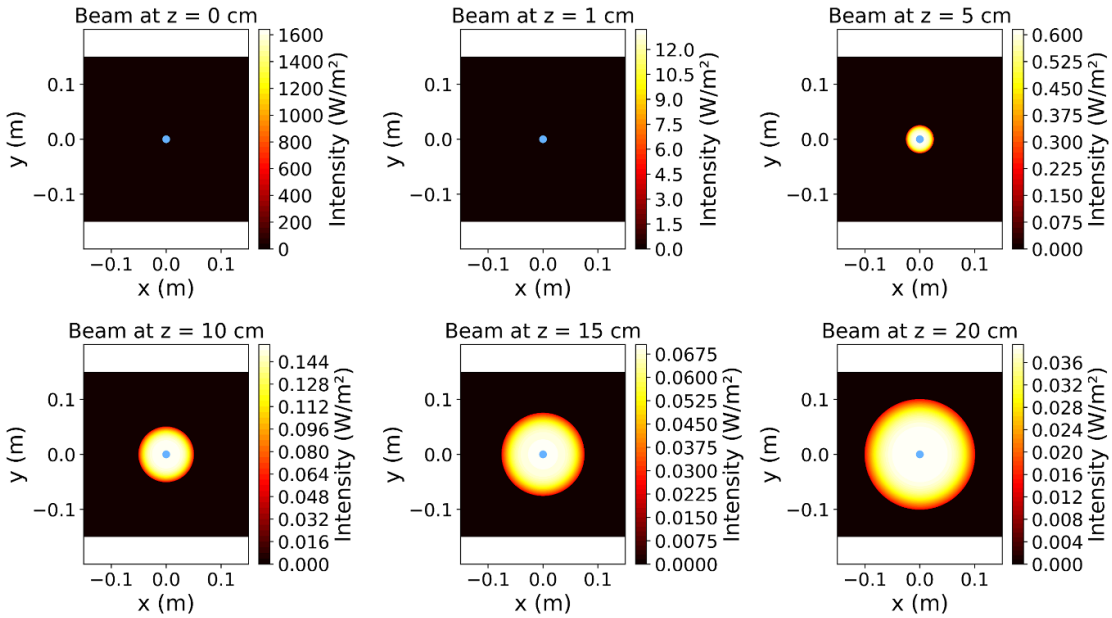

Figure 5. Light intensity distribution at various distances z from the N = 1 optical fiber sample (detector area: blue circle).

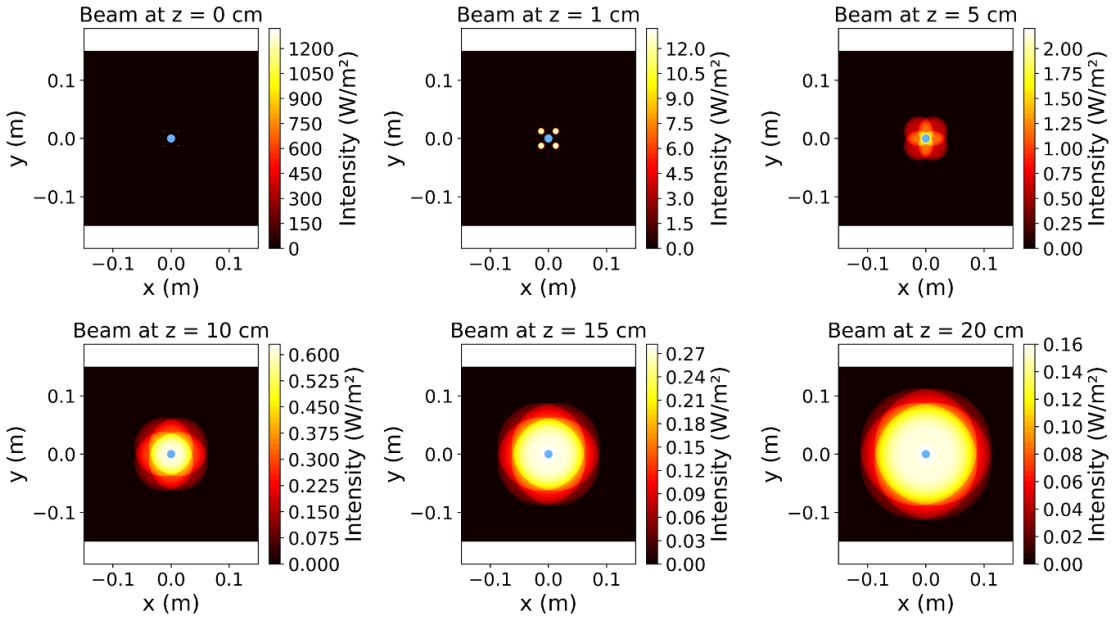

Figure 6. Light intensity distribution at various distances z from the N = 4 optical fiber samples (detector area: blue circle).

nine fibers to expand, resulting in greater overlap of their profiles. Thus, determining the optimal distance requires balancing light capture across the entire fiber array, accounting for both the central and surrounding fibers.

For the $N = 16$ fibers configuration, the center-aligned detector can capture light cones from the four innermost fibers at shorter distances ($z < 5$ cm), most effectively. However, to maximize light capture from all 16 fibers, including the twelve fibers positioned along the sample's periphery, the detector needs to be placed at a greater distance. As the detector is moved further away from the sample, the light cones from each fiber expand, again enhancing the overlap among their profiles as well as a more uniform intensity distribution (figure 8).

The beam profile analysis across varying distances and fiber configurations demonstrates the influence of fiber arrangement on light distribution and detection efficiency. For single-fiber setups, closer

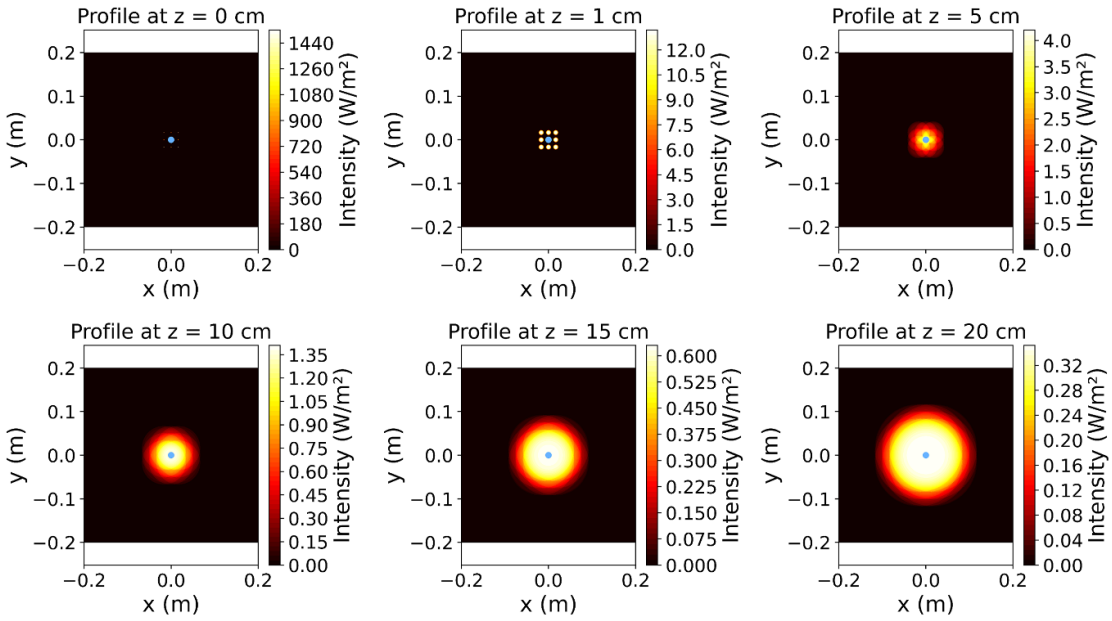

Figure 7. Light intensity distribution at various distances z from the N = 9 optical fiber samples (detector area: blue circle).

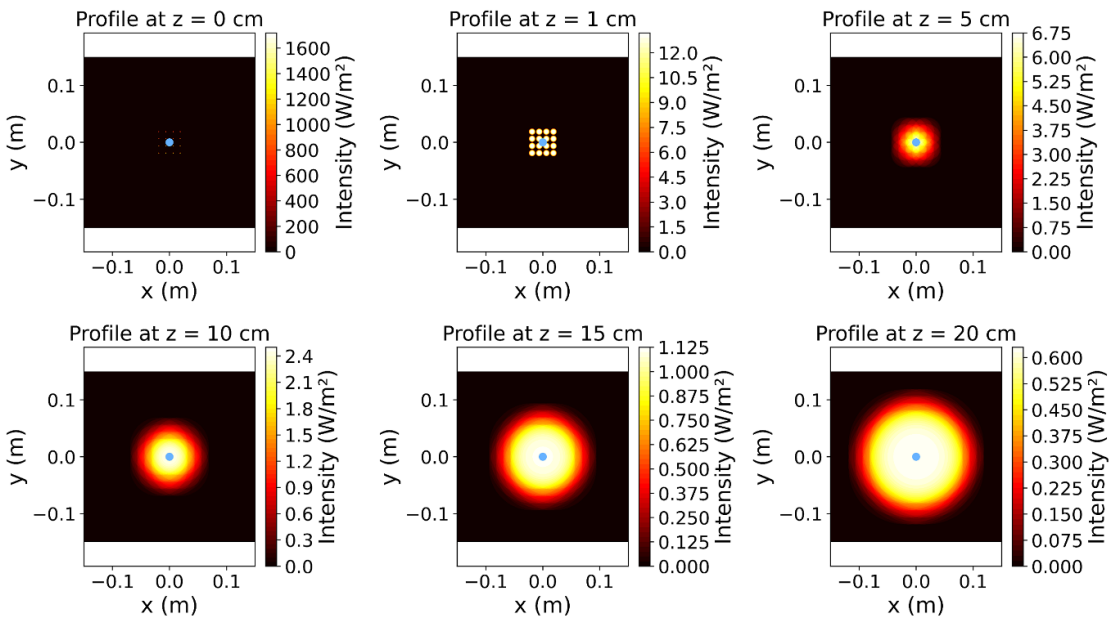

Figure 8. Light intensity distribution at various distances z from the 16 optical fiber samples (detector area: blue circle).

detector positioning maximizes light capture. Conversely, in multi-fiber configurations, the detection distance must be optimized to account for the overlap of light cones with the detector area, ensuring efficient capture of light from all fibers while maintaining sufficient intensity.

The experimental results, presented in figure 9, provide a quantitative analysis of transmittance as a function of detection distance, fiber quantity, and light source. Each plot depicts transmittance (%) for different fiber quantities ($N = 1, 4, 9, 16$ fibers) across detection distances of $z = 1, 2, 5, 10, 15$, and 20 cm. The analysis is performed with two types of visible light sources (LED white light bulbs and RGB LEDs), which represent commonly used types of ambient illumination sources. Additionally, the dashed lines in figure 9, indicate the highest theoretical transmittance that the samples could achieve based on the model described in the previous section. These theoretical curves (i.e. dashed lines in figure 9) were calculated using equation (2) and serve as a reference for evaluating the experimental results, providing a benchmark for understanding the efficiency of light transmission across the different fiber configurations.

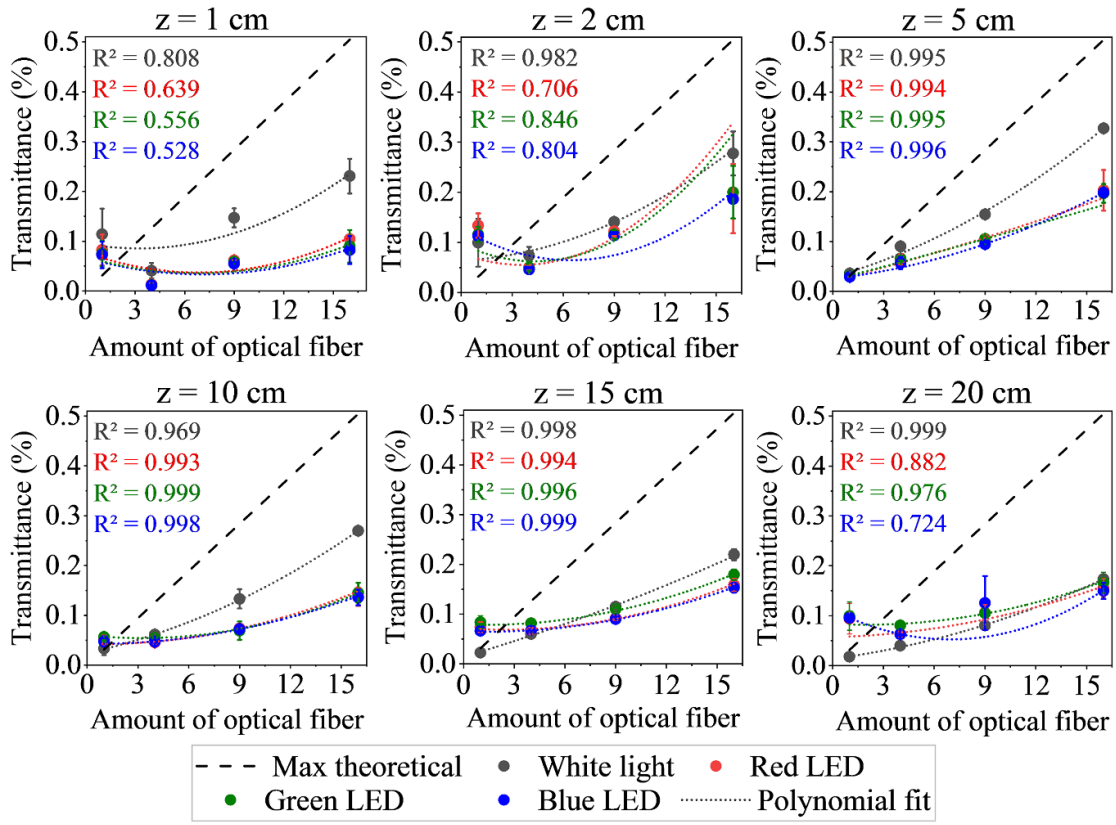

Figure 9. Measured light transmittance (%) in LTC samples as a function of fiber quantity and detector-distance (z) for each light source.

The discrepancy between the experimental transmittance values and the theoretical maximum predicted by the model can be attributed to several factors. First, imperfections in fiber cleaving can reduce light coupling efficiency [13]. Second, the model assumes ideal conditions, such as a defect-free fiber and a perfectly stable light source, which do not fully reflect experimental conditions. Additionally, the model does not account for the acceptance angle of the fibers, which limits the amount of light that can be effectively guided [15]. The variability across measurements remained low, with standard deviations from 0.000% to 0.013%, which indicates consistent behavior between the two specimens tested for each configuration.

Furthermore, the model assumes ideal fiber alignment. While the fibers are threaded through precision-drilled plates to minimize misalignment, any minor deviation from the longitudinal axis can result in an asymmetric output beam. Additionally, while the matrix is largely opaque, internal reflections at the fiber-matrix interface or scattering from minor surface imperfections near the fiber exit could introduce small deviations [40].

The increase in the number of fibers generally leads to higher transmittance across all detection distances, and also show that additional fibers enhance the overall transparency of LTC samples as expected [12–15, 41]. For instance, at a detection distance of 1 cm with the white light source, transmittance rises from 0.11% with 1 fiber to 0.23% with 16 fibers—an approximate 102% increase. This trend of rising transmittance with more fibers persists at 20 cm, where transmittance reaches 0.17% for 16 fibers compared to 0.02% with 1 fiber, representing a 9-fold improvement. These results confirm that adding fibers consistently improves light transmission regardless of distance, though the absolute effect is more pronounced at shorter distances where light remains more concentrated [28]. Interestingly, in certain configurations, such as the 1-fiber setup, experimental results occasionally exceed the maximum theoretical transmittance at specific detection distances. This unexpected result could arise from experimental factors such as light scattering and leakage, or temporal fluctuations in light source power.

The 4-fiber configuration presents a distinct trend, with lower transmittance than the 1-fiber setup at shorter detection distances, particularly at 1 cm and 2 cm (0.04% and 0.07% respectively, for the white light source). This behavior is due to the fiber distribution, with the center of the sample lacking fibers. When the detector is positioned very close to the sample, it captures less light from the light cones of

the peripheral fibers, resulting in reduced transmittance, as previously discussed in the beam profile analysis. However, from 5 cm onward, the detector is positioned far enough to capture more light from the peripheral fibers, leading to higher transmittance for the 4-fiber configuration (0.09% at 5 cm). These findings suggest that while increasing fiber count generally benefits transmittance, fiber distribution and spacing, is important in optimizing illumination from LTC [15, 17, 20, 42].

For the 9-fiber configuration, transmittance values varied from 0.08% to 0.15% across the detection distances tested. At a short distance of 1 cm, transmittance reached 0.14%, reflecting effective light capture due to the proximity between the detector and the central fiber in the specimen. A slight decrease to 0.13% was observed at 10 cm, followed by a more pronounced reduction to 0.08% at 20 cm. This behavior can be attributed to the diminishing light intensity with increasing distance, as the emitted light becomes more dispersed over a larger area [14, 19, 24]. The peak transmittance of 0.15% at 5 cm suggests that this intermediate distance allows for an optimal balance of light detected from the distributed fibers.

For the 16-fiber configuration, transmittance varied from 0.17% to 0.33%, with the highest value recorded at 5 cm. The increased fiber quantity enhanced light transmission across all distances. This is consistent with the denser fiber arrangement (6.25 mm spacing), which promotes higher light overlap, as illustrated in figure 8. Interestingly, the results for the 16-fiber setup concur with findings by Chiew *et al* [15], who reported a transmittance of approximately 0.2% for $10 \times 10 \times 10$ cm samples containing the same amount and diameter of fibers spaced 2.5 cm apart, at a detection distance of 10 cm. Despite the larger sample size in their study, the comparable transmittance values highlight the effectiveness of the compact fiber arrangement used here.

As has been well established, distance detection significantly influences transmittance behavior. At shorter detector distances, such as $z = 1$ cm and 2 cm, results in figure 9 indicate an irregular behavior for configurations with low number of fibers (e.g., $N < 9$) because the detector is too close to the LTC sample, resulting in a sporadic overlap of the detector with the non-homogeneous light distribution. In contrast, at an intermediate detection distance of $z = 5$ cm, the light cones from each fiber expand sufficiently to allow a somewhat homogeneous light distribution to overlap with the detector, irrespective of the number of fibers in the sample. The distance aligns with the hypothesis, where the spatial arrangement provides the most balanced and representative power measurements. This results in a balanced transmittance distribution and optimal values for most configurations. As shown by the theoretical maximum transmittance line (figure 9), the transmittance at this distance ($z = 5$ cm) approaches the calculated upper theoretical limits more closely than at other distances across different fiber quantities for the LTC samples used in this study, validating the methodological importance of the geometric overlap effect.

As the detection distance extends beyond 10 cm, a marked decline in transmittance occurs across all configurations, primarily due to increased light attenuation over longer distances. At these greater distances, light disperses further, diminishing the direct capture potential of the detector and spreading the light beyond the detector's effective area [15, 24]. Although the rate of transmittance reduction is most pronounced between 1 cm and 10 cm, it begins to stabilize beyond 10 cm, indicating that the dispersion effect has a diminishing impact as the distance further increases, as was also reported by Rong *et al* [24]. For instance, the transmittance drop between 5 cm and 20 cm is notably smaller than the initial decline, showing that while detected light decreases with distance, the dispersion effect attenuates more gradually over extended ranges.

The type of light source can also influence the transmittance behavior [19]. In figure 9, the white light source generally demonstrates slightly higher transmittance across all configurations. For instance, at 1 cm, the white light source achieves a transmittance of 0.11% with a single fiber, whereas the red LED reaches 0.08%. Similarly, with 16 fibers, the white light source attains 0.23%, while the maximum transmittance for the LED sources is limited to around 0.1%. This small difference in the measured transmittances between the LED white light bulb and RGB LED sources can be attributed to the light source directionality, which is different. In fact, the LED sources include a small collimating lens that helps create a more directional incident light source, compared to the LED bulb. Moreover, the higher optical power of the white LED (6 W vs 3 W) likely improves the signal-to-noise ratio, while its broad spectral distribution ensures better overlap with the spectral responsivity of the S142C integrating sphere detector. Hence, the choice of the types of light sources used in LTC transmission assessments is another way to better model artificial and natural lighting conditions.

A quantitative analysis of the light sources confirms that wavelength-dependent effects are negligible at the scale of the specimens used in this study. Using the fiber attenuation data (200 dB km^{-1} at 650 nm), the calculated intrinsic loss through a 5 cm specimen is less than 0.2 %, ensuring that spectral filtering by the fiber does not significantly affect the measured transmittance [43, 44]. Additionally,

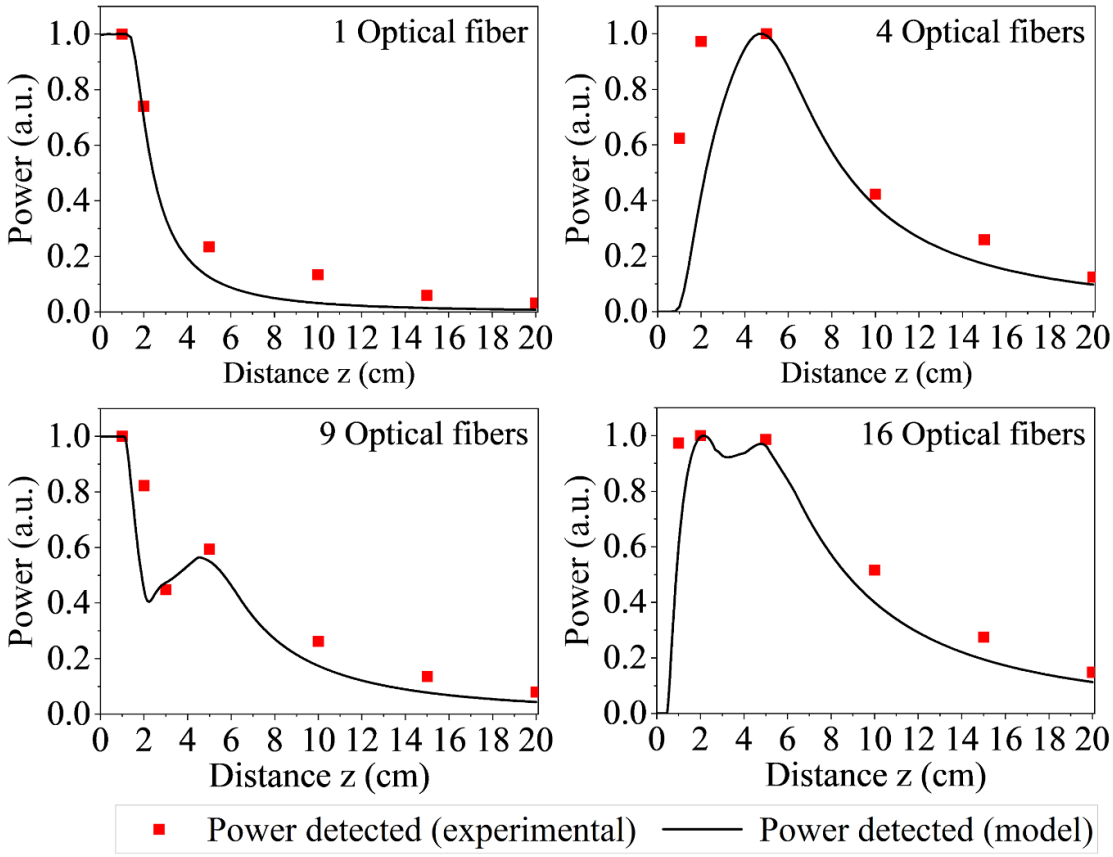

Figure 10. Comparison of detected power versus detector distance z between experimental measurements and theoretical model predictions for all fiber configurations (N = 1, 4, 9, 16).

since the NA of PMMA fibers varies minimally across the visible spectrum, the beam divergence angle (θ) remains effectively constant. Consequently, the practical estimation model, parameterized using white light, remains applicable to the LED RGB sources, since the geometric propagation of light is the dominant factor that determines the power detected as a function of distances.

3.2. Optimal detection distance and model validation

The experimental validation was performed by directly comparing the normalized experimental data with the theoretical predictions (figure 10). Specifically, the model integrates the optical intensity of the overlapping super-Gaussian beams over the 12 mm circular area of the photodetector, as defined in equations (3) and (4). By explicitly matching the detector aperture in the mathematical formulation, the model enables a direct spatial correspondence between the simulated and measured detected power at each discrete detector-sample distance z. The simulations assumed an input optical power of 1 mW (at 550 nm wavelength) injected into each N optical fibers. The selected wavelength of 550 nm, located in the green region, serves as an average value within the visible spectrum (roughly between 400–700 nm), and was chosen to align the theoretical predictions with the broad-spectrum measurements performed using the experimental light sources. The model also incorporates parameters such as the NA of the optical fiber and super-Gaussian parameter $n = 3$, both of which inform light propagation through the fiber network [7, 22, 45].

The detected light power at distances from $z = 0$–20 cm (relative to the sample's center) was thus simulated for the different sample configurations with $N = 1$, 4, 9, and 16 fibers. Figure 10 presents the detected power in the model simulations (solid curves) with the experimentally measured power (red markers). To facilitate comparison, both results were unit-normalized to ensure they are presented on the same scale.

As shown in figure 10, both experimental and theoretical model curves of power detection exhibit similar behaviors, indicating the model's effectiveness in accurately describing the experimental conditions of light transmission in fiber-based LTC samples. As suggested earlier, for the 1-fiber configuration there is no obvious optimal detection distance. Because there is only one fiber that is centrally positioned and aligned with the detector, the detected power simply falls off with the distance. Here, a

practical issue would be not to place the detector too close to the sample so as to not saturate the photodetection signal.

For the 4-fiber configuration, the detection profile shows a different behavior. At very short distances ($z = 0$), the model predicts no detectable power, as expected, since there is no fiber in the center of the sample in this configuration. Yet, experimental data indicated a small detectable power at a short $z = 1$ cm distance, which is likely due to factors such as noise, calibration errors or potential light leakage in the setup. Notably, the model's prediction of peak power detection occurring around 5 cm is validated by the experimental data.

For the 9-fiber configuration, the detected power exhibits a more complex profile due to the geometric distribution of the fibers. At short distances ($0 \leqslant z \leqslant 1$cm), the detected signal is dominated by the central fiber, while at larger distances the contribution from the surrounding fibers becomes increasingly significant. This transition results in a non-monotonic detection profile, with an initial high detected power, followed by a decrease and a subsequent secondary increase at larger z values. Due to this more complex behavior associated with fiber geometry, an additional experimental measurement point at $z = 3$ cm was included in the analysis, allowing a more accurate characterization of the transition region between central-fiber dominance and collective multi-fiber detection. Despite the increased complexity, both the model and experimental data indicate a consistent optimal detection distance close to $z \approx 5$ cm.

For the 16-fiber configuration, the model predicts two distinct peaks in the power detection profile. The first peak, around 2 cm, is ascribed to the power contribution of the four innermost fibers (see the $z = 1$ cm sub-figure in figure 8). This is followed by a small 'valley' in detected power in the $2 \leqslant z \leqslant 4$cm region as the detector moves away from the innermost fibers. A second detection peak appears at $z = 5$ cm owing to the additional intensity contribution of the 12 outermost fibers to the total detected power (see the $z = 5$ cm sub-figure in figure 8). Hence, the detector location at $z = 5$ cm enables to 'sample' the light cones emitted by all 16 fibers of this configuration. The presence of the secondary peak is validated by the experimental data.

Furthermore, both experimental data and the model show stabilization in optical power detection at larger distances ($z > 14$ cm) as well as the exponential decay. This stability indicates that the system reaches a limit in its detection capacity beyond this point, as further increases in distance do not result in significant detected power [24, 28, 29].

3.3. Practical estimation of optimal sample-detector distance

The comparison between experimental results and the model's predictions (figure 10) provides valuable insights. While existing studies have empirically analyzed the influence of fiber arrangement and detector distance for various configurations of fibers and LTC samples [12, 24, 28, 29], as far as we know, there is no general rule available to researchers on the optimal location of a small photodetector with respect to the LTC sample in order to obtain a reliable assessment of light transmittance via optical power measurements. In this regard, we propose a simple estimation method to determine such an optimal sample-detector distance.

This estimation provides a practical tool for experimental planning, allowing researchers to determine the most effective setup for power detection, which takes into account the dimensions of the LTC sample under study and the NA of the optical fibers embedded in the sample. The NA is related to how wide light spreads as it exits the fiber, $\mathrm{NA} = \sin(\theta)$, where θ is the half-angle of the emitted light cone [45].

The optimal detection distance, z_{opt}, can be practically estimated based on the characteristic dimension of the sample, D_{s}, which represents the largest dimension of the LTC sample. For square samples, as in the current work, D_{s} corresponds to the side length. For non-square samples, D_{s} should be taken as the longest side facing the detector, as this dimension most significantly influences light transmission from the N fibers that are assumed to be uniformly distributed throughout the entire output surface of the sample. Figure 3 illustrates the light cones emitted by two optical fibers and their overlapping intensity distributions. Considering the extreme situation where two such light-emitting fibers, located at the opposite ends on the outer periphery of the sample (i.e., therefore spaced apart by approximately D_{s}), the optimal detection distance should correspond to the $z = z_{\mathrm{opt}}$ value at which their intensity distributions begin to overlap at the detector's location. This geometric criterion is met when the radius of the expanding cone R, defined by $r = z \times \tan(\theta)$, is equal to half of the characteristic sample dimension ($D_s/2$). Based on the considerations shown in figure 3, a simple estimation of z_{opt} can thus be derived as equation (5), where the small-angle approximation was used for the definition of the fiber's $\mathrm{NA} = \sin\theta \propto \tan\theta$,

$$z_{\mathrm{opt}} \propto \frac{D_S/2}{\tan\theta} \approx \frac{D_S}{2 \cdot NA}\,. \tag{5}$$

The estimation in equation (5) reflects a geometric overlap criterion. Changes in fiber diameter affect signal amplitude, whereas the optimal distance occurs from the NA and the sample geometry. For the experimental setup of this study, the sample size is $D_s = 5$ cm and the fiber NA = 0.5, such that the estimated optimal distance (using equation (5)) to place the detector away from the center of the sample is $z_{opt} = 5$ cm. This estimation value, obtained for the specific LTC sample dimensions and PMMA fibers used in this experiment agrees with the trends presented in figures 9 and 10, and aligns well with empirical findings reported in the broader literature, where detector placement has historically been determined experimentally rather than analytically.

For instance, Rong *et al* [24] investigated light transmittance in LTC panels ($30 \times 40 \times 7.5$ cm^3) using 2 mm diameter PMMA optical fibers arranged in 5×5 and 6×6 grid configurations (300 and 432 fibers, respectively). In their experimental configuration, the optimal light intensity occurred with the light source at 20 cm, and the detector was placed between 30 and 40 cm from the sample. Given the use of PMMA optical fibers, the NA can be reasonably assumed to be close to 0.5. Consequently, the reported optimal detection distance range aligns with the trend predicted by the practical estimation model (equation (5)) proposed in this work. Using a comparable setup, Nam *et al* [14] studied light transmittance in $10 \times 10 \times 5$ cm^3 rectangular LTC samples, using polymer optical fibers with diameters of 0.75, 1.0, and 1.5 mm at various spacings. The highest light transmittance was measured at 10 cm, with intensity decreasing as the distance increased (20–30 cm). While the NA of the fibers was not provided, the use of PMMA fibers suggests a NA similar to that adopted in the present study. Under this condition, the optimal detection distance of 10 cm, would be in agreement with the definition of the estimated optimal distance proposed in this study.

Additionally, Li *et al* [12] investigated light transmittance through LTC samples with dimensions of $4 \times 8 \times 1$ cm^3, containing PMMA optical fibers of 0.5 and 1 mm in diameter. Their results showed a decrease in detected power as the distance between the detector and the sample increased, from 10 cm to 40 cm. Assuming a comparable NA of 0.5 associated with PMMA fibers, our model predicts an optimal detection distance of 8 cm for their sample dimensions. Although their measurements began at 10 cm, the observed trend of decreasing transmittance with increasing distance aligns with the general behavior predicted by the model presented in this study. A similar pattern is evident in the work of Tuaum *et al* [29], who studied 10 cm cubic specimens. They measured intensity using a light-dependent resistor at distances from 10 to 50 cm and noted a progressive decrease in intensity following the general distance-dependent trend predicted by our model. Our model suggests an optimal distance closer to 5 cm for this configuration. Thus, the monotonic decrease observed from 10 cm onwards is consistent with a peak intensity located at a shorter distance than their starting measurement point.

Additionally, Chiew *et al* [15] investigated light transmittance in cubic specimens of 10 cm, using optical fibers with a diameter of 1 mm and an NA of 0.51, arranged with 25 mm spacing. Light transmittance was measured at a detection distance of 10 cm. Despite not focusing on testing different detection distances, the 10 cm measurement aligns closely with the optimal distance predicted by the proposed practical estimation model presented in this study for similar sized samples. Finally, Tahwia *et al* [46] evaluated translucent self-compacting concrete specimens ($10 \times 10 \times 10$ cm^3) with 1 and 2 mm PMMA fibers, measuring at distances from 0 to 40 cm. Although transmittance decreased with distance, values at 10 cm were very close to those at zero distance and significantly higher than at larger distances. This observation further validates the present simplified model, which identifies the 5–10 cm range as the optimal region for stable transmission measurements in samples of this geometry.

Figure 11 summarizes detector-sample distances reported in the literature alongside the optimal distance estimated and experimentally validated in this study. A linear relationship is observed between sample size, from 4×8 cm^{-2} to 30×40 cm^2, and the optimal detector distance across fiber diameters from 0.5 to 3 mm. This behavior is expected since most commercial PMMA fibers exhibit similar NAs ($\sim$0.5), leading to comparable beam divergence independently of core diameter. These studies did not aim to determine an optimal detector-sample distance, and measurements were generally performed at fixed or limited distances based on their experimental setups. For instance, the value plotted for Rong *et al* [24] represents the midpoint of their reported 30–40 cm optimal distance range. The reported values are therefore presented here for comparative trend analysis rather than as claimed optima. Despite variations in sample dimensions, fiber diameters, and experimental setups, the reported distances fall within or close to the range predicted by the proposed estimation model.

Despite the range of fiber diameters considered in the literature, the scaling of the optimal detector distance with sample size remains consistent, indicating that the optimal distance is controlled by angular spreading rather than by the emitting core size. While this estimation offers a simplified and practical guideline, the theoretical model (equations (3) and (4) developed in this study provides a physically

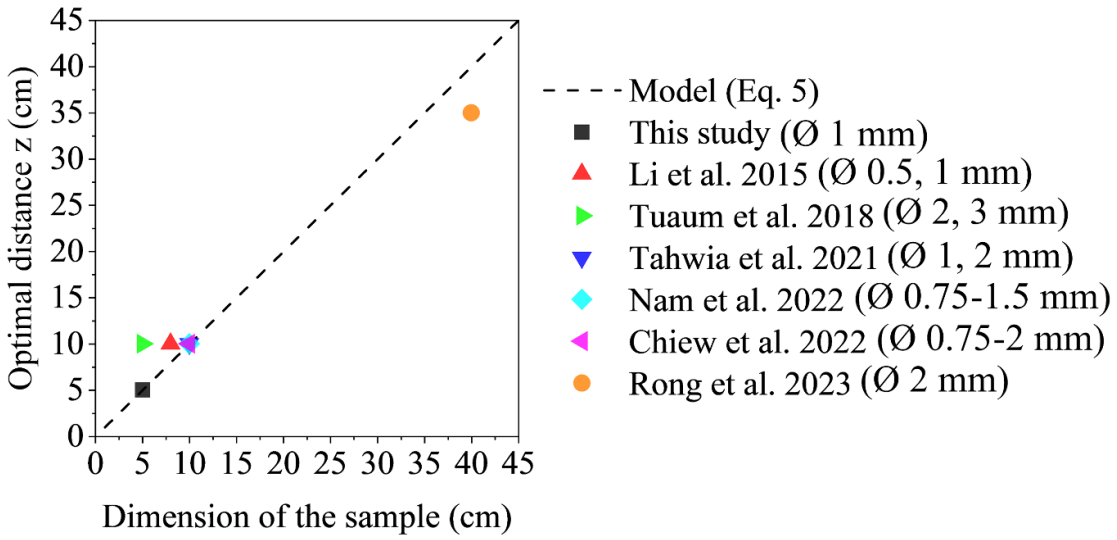

Figure 11. Comparison between the optimal detector-sample distance predicted by the practical estimation model (dashed line) and literature-reported detector-sample distances for PMMA-based light-transmitting concrete (symbols), for specimen dimensions from 4 × 8 cm^2 to 30 × 40 cm^2 and fiber diameters between 0.5 and 3 mm.

grounded framework for performing a detailed analysis and optimization of light transmission measurements in fiber-based LTC samples, incorporating the specific influence of sample geometry and fiber characteristics.

4. Conclusions

This study examined light transmission in LTC using an experimental framework combined with a super-Gaussian description of the emitted light field. The work evaluated the influence of fiber quantity, detector-sample distance, and light source type on measured transmittance. A simplified estimation model based on sample dimensions and fiber NA was also proposed and validated. The model reliably predicted the detected power trends observed experimentally. The key findings are:

- Fiber quantity: higher numbers of embedded fibers improved light transmittance by broadening and homogenizing the intensity distribution. Configurations with 16 fibers consistently showed the highest transmittance.
- When expressed relative to the characteristic sample dimension D_s, the detector-sample distance z defines distinct transmittance regimes. Short distances, between 0.2 D_s and 0.4 D_s, favor the detection of centrally aligned fibers. Intermediate distances, on the order of D_s, promote overlap of the emitted light cones and result in maximum transmittance across all configurations. At larger distances, greater than approximately 1.5 D_s, attenuation and beam dispersion dominate, with a stabilization trend observed for distances exceeding 2 D_s.
- Light source: for this experiment, the white light produced slightly higher transmittance at short distances compared to RGB LEDs, while differences diminished at longer distances.
- Model validation: both the super-Gaussian framework and the practical (simplified) estimation model accurately predicted experimental trends and optimal detector placement.

The proposed estimation approach and theoretical model, while developed for 1 mm PMMA fibers, apply to other fiber diameters and materials, as they primarily depend on the fiber NA. This study establishes a standardized measurement protocol for LTC optical characterization, enabling reproducible evaluation of fiber-based cementitious composites. Future work may extend the framework to larger experimental datasets, alternative fiber materials, and optically active or smart cement-based applications.

Acknowledgments

This research was funded by the Fonds de Recherche du Québec Nature et Technologies through Grant Number 370841 (https://doi.org/10.69777/370841) and the Art Prisme programme (2022-ART-317342), Canada research chair of sustainable multifunctional materials (CRC-2019-00074), and ÉTS Research chair in engineering Marcelle-Gauvreau.

Data availability statement

All data that support the findings of this study are included within the article (and any supplementary files).

Conflict of interest

The authors declare no known competing financial interests or personal relationships that could have influenced the work reported in this paper.

Author contributions

Karina Hwang Arcolezi 0000-0001-5308-5747
Conceptualization (lead), Data curation (lead), Formal analysis (lead), Funding acquisition (supporting), Investigation (lead), Methodology (lead), Validation (lead), Visualization (lead), Writing – original draft (lead), Writing – review & editing (lead)

Camila Aparecida Zimmermann 0000-0001-9573-0900
Data curation (supporting), Formal analysis (supporting), Writing – review & editing (supporting)

Bora Ung 0000-0003-1046-9489
Conceptualization (supporting), Data curation (supporting), Formal analysis (supporting), Funding acquisition (lead), Investigation (supporting), Methodology (supporting), Project administration (lead), Resources (lead), Supervision (lead), Validation (equal), Visualization (supporting), Writing – review & editing (supporting)

Claudiane Ouellet-Plamondon 0000-0003-3795-4791
Conceptualization (supporting), Data curation (supporting), Formal analysis (supporting), Funding acquisition (lead), Investigation (supporting), Methodology (supporting), Project administration (lead), Resources (supporting), Supervision (lead), Validation (supporting), Visualization (supporting), Writing – review & editing (supporting)

References

[1] Chiew S M, Ibrahim I S, Mohd Ariffin M A, Lee H-S and Singh J K 2023 Assessment and ANN model development of natural light transmittance of light-transmitting concrete *Results Eng.* **20** 101416
[2] Luhar I, Luhar S, Savva P, Theodosiou A, Petrou M and Nicolaides D 2021 Light transmitting concrete: a review *Buildings* **11** 480
[3] Said S H 2020 State-of-the-art developments in light transmitting concrete *Mater. Today Proc.* **33** 1967–73
[4] Shen J and Zhou Z 2013 Some progress on smart transparent concrete *Pac. Sci. Rev.* **15** 51–55
[5] Chiew S M, Ibrahim I S, Sarbini N N, Ariffin M A M, Lee H S and Singh J K 2020 Development of light-transmitting concrete—A review *Mater. Today Proc.* **39** 1046–50
[6] Ahuja A and Mosalam K M 2017 Evaluating energy consumption saving from translucent concrete building envelope *Energy Build* **153** 448–60
[7] Su X, Zhang L, Luo Y and Liu Z 2022 Energy & buildings an energy analysis of translucent concrete embedded with inclined optical fibers *Energy Build* **273** 112409
[8] Navabi D, Amini Z, Rahmati A and Tahbaz M 2023 Developing light transmitting concrete for energy saving in buildings *Case Stud. Constr. Mater.* **18** e01969
[9] Shen J and Zhou Z 2021 Light transmitting performance and energy-saving of plastic optical fibre transparent concrete products *Indoor Built Environ.* **30** 635–49
[10] Inaudi D, Posenato D and Glisic B 2005 Combined static and dynamic monitoring of civil structures with long-gauge fiber optic sensors *23rd Int. Modal Analysis Conf.* (*Florida*)
[11] Arcolezi K H, Marion V, Ung B and Ouellet-Plamondon C 2025 Randomly distributed optical fibers in translucent mortar for privacy-preserving light transmission and digital image reconstruction *Sci. Rep.* **16** 2454

[12] Li Y, Li J and Guo H 2015 Preparation and study of light transmitting properties of sulfoaluminate cement-based materials *Mater. Des.* **83** 185–92
[13] Henriques T D S, Dal Molin D C and Masuero Â B 2018 Study of the influence of sorted polymeric optical fibers (POFs) in samples of a light-transmitting cement-based material (LTCM) *Constr. Build. Mater.* **161** 305–15
[14] Nam H P, Hai N M, Van Huong N, Quang P D, Tuan N D, Hai D V, Binh N T and Vy T Q 2022 Experimental study on 80 MPa grade light transmitting concrete with high content of optical fibers and eco-friendly raw materials *Case Stud. Constr. Mater.* **18** e01810
[15] Mei Chiew S, Syahrizal Ibrahim I, Azreen Mohd Ariffin M, Lee H-S and Kumar Singh J 2022 Evaluation of light transmittance performance of light-transmitting concrete with optical fibre *Constr. Build. Mater.* **351** 128949
[16] Altlomate A, Alatshan F, Mashiri F and Jadan M 2016 Experimental study of light-transmitting concrete *Int. J. Sustain. Build. Technol. Urban Dev.* **7** 133–9
[17] Shenoy A, Nayak G, Tantri A and Shetty K K 2022 Thermal transmission characteristics of plastic optical fibre embedded light transmitting concrete *Mater. Today Proc.* **65** 1759–73
[18] Pourkazemi M, Vahdati M, Mirvalad S and Mahdikhani M 2024 Light-transmitting concrete: performance and novel casting methods *Constr. Build. Mater.* **449** 138270
[19] Li Y, Li J, Wan Y and Xu Z 2015 Experimental study of light transmitting cement-based material (LTCM) *Constr. Build. Mater.* **96** 319–25
[20] Sharifi S, Navabi D and Mosavi A 2023 Translucent concrete: comprehensive review of concepts, recent technologies and advances in light transmitting concrete *2023 IEEE 17th Int. Symp. on Applied Computational Intelligence and Informatics (SACI)* (IEEE) pp 000685–92
[21] Huang B 2020 Light transmission performance of translucent concrete building envelope *Cogent Eng.* **7**
[22] Su X, Zhang L, Liu Z, Luo Y, Lian J and Liang P 2020 Daylighting performance simulation and analysis of translucent concrete building envelopes *Renew. Energy* **154** 754–66
[23] Tahwia A M, Abdelaziz N, Samy M and Amin M 2022 Mechanical and light transmittance properties of high-performance translucent concrete *Case Stud. Constr. Mater.* **17** e01260
[24] Rong T C, Mei C S, Mohammed Al-Fasih M Y, Ibrahim I S, Sarbini N N and Padil K H Light-transmitting concrete properties of short wall panel *ASEAN Eng. J.* **13** 109–17
[25] Štochl N, Vychytil J and Hájek P 2023 Illumination of interior spaces through structures made of unified slabs of high-performance light-transmitting concrete with embedded optical Fibers *Materials* **16** 3142
[26] Henriques T D S, Dal Molin D C and Masuero Â B 2020 Optical fibers in cementitious composites (LTCM): analysis and discussion of their influence when randomly arranged *Constr. Build. Mater.* **244** 118406
[27] Bai J, Zhang W, Tian J, Wu X and Zheng M 2024 Development of optical fiber light-transmitting concrete (LTC)—A review *Buildings* **15** 104
[28] Robles A, Arenas G F and Stefani P M 2020 Light transmitting cement-based material (LTCM) as a green material for building *J. Appl. Res. Technol. Eng.* **1** 9
[29] Tuaum A *et al* 2018 Experimental evaluation on light transmittance performance of translucent concrete *Int. J. Appl. Eng. Res.* **13** 1209–18
[30] Shealy D L and Hoffnagle J A 2005 Beam shaping profiles and propagation *Proc. SPIE* **5876** 58760D
[31] Rativa D and Vohnsen B 2011 Single- and multimode characteristics of the foveal cones: the super-Gaussian function *J. Mod. Opt.* **58** 1809–16
[32] Canadian Standards Association—CSA A3000: cementitious materials compendium (2018)
[33] Arcolezi K H, Ung B and Ouellet-Plamondon C 2024 Influence of optical fibres on mechanical properties of mortar mixes *To Appear Canadian Society for Civil Engineering Annual Conf.* (*Niagara Falls, Canada*)
[34] Jin W, Caron J-F and Ouellet-Plamondon C M 2025 Minimizing the carbon footprint of 3D printing concrete: leveraging parametric LCA and neural networks through multiobjective optimization *Cem. Concr. Compos.* **157** 105853
[35] Alonso Romero A, Amouzou K N, Sengupta D, Zimmermann C A, Richard-Denis A, Mac-Thiong J-M, Petit Y, Lina J-M and Ung B 2023 Optoelectronic pressure sensor based on the bending loss of plastic optical fibers embedded in stretchable polydimethylsiloxane *Sensors* **23** 3322
[36] Navabi D, Javidruzi M, Hafezi M R and Mosavi A 2021 The high-performance light transmitting concrete and experimental analysis of using polymethylmethacrylate optical fibers in it *J. Build. Eng.* **38** 102076
[37] Gillen-Christandl K, Gillen G D, Piotrowicz M J and Saffman M 2016 Comparison of Gaussian and super Gaussian laser beams for addressing atomic qubits *Appl. Phys. B* **122**
[38] Belay G Y *et al* 2022 Dynamic optical beam shaping system to generate Gaussian and top-hat laser beams of various sizes with circular and square footprint for additive manufacturing applications *Proc. CIRP* **111** 75–80
[39] Yoshizaki R and Nakao M 2023 Ultrashort pulse laser processing of single crystalline diamond for efficient and smooth grooving with top-hat beam modulation *CIRP Ann.* **72** 189–92
[40] Mbabazi J, Luo Z, Du Q, Wang Y and Lyu Q 2026 Light-transmitting foamed concrete composites with tailored mechanical-optical-thermal functionality *J. Build. Eng.* **119** 115202
[41] Sawant A B *et al* 2014 Light transmitting concrete by using optical fiber *Int. J. Inventive Eng. Sci.* **3** 23–8
[42] Shenoy A, Nayak G, Tantri A, Shetty K K and Mahesha M G 2025 Characterization of light-transmitting concrete incorporating bundled optical fibres *Innov. Infrastruct. Solut.* **10** 8
[43] Hai N M, Quang P D and Nam H P 2025 Evaluation of lighting energy savings and embodied carbon of light-transmitting concrete incorporating polymethyl methacrylate for building envelopes *J. Build. Eng.* **112** 113807
[44] Lian F and Yin Z 2022 Mechanical, light transmittance properties and simulation study of sustainable translucent lightweight aggregate concrete *Mater. Res. Express* **9** 025507
[45] Su X, Zhang L, Liu Z, Luo Y, Liang P and Lian J 2022 An optical and thermal analysis of translucent concrete considering its dynamic transmittance *J. Clean. Prod.* **364** 132588
[46] Tahwia A M, Abdel-Raheem A, Abdel-Aziz N and Amin M 2021 Light transmittance performance of sustainable translucent self-compacting concrete *J. Build. Eng.* **38** 102178